Hindawi Publishing Corporation
Advances in Power Electronics
Volume 2013, Article ID 261959, 7 pages
http://dx.doi.org/10.1155/2013/261959

Research Article

Transformer Magnetization Losses Using a Nonfiltered Voltage-Source Inverter

Rickard Ekström, Senad Apelfröjd, and Mats Leijon

Division for Electricity, Swedish Centre for Renewable Electric Energy Conversion, Uppsala University, P.O. Box 534, 751 21 Uppsala, Sweden

Correspondence should be addressed to Rickard Ekström; rickard.ekstrom@angstrom.uu.se

Received 17 December 2012; Accepted 9 April 2013

Academic Editor: Jose Pomilio

Results from the magnetization of an 80 kVA power transformer, using a directly coupled nonfiltered three-phase voltage-source inverter (VSI), are presented. The major benefits of this topology are reduction in switching filter size as well as filter losses. Drawbacks include higher stress on the transformer windings and higher transformer magnetization losses. In this paper, the total magnetization losses are presented for different voltage levels. The transformer has been magnetized with the rated frequency of 50 Hz at various voltage levels. The saturation characteristics as well as the magnetizing resistance are derived as functions of the voltage. These are used as inputs for the simulations. The magnetization losses have been experimentally measured and simulated for three different DC levels. Results from the simulations show good agreement with the experimental results. As expected, the pulsed voltage waveforms generate larger magnetization losses than the corresponding 50 Hz case. The losses are strongly dependent on the DC level.

1. Introduction

Many grid connected voltage source inverters (VSIs) have an associated LCL filter to eliminate the switching frequencies from the output [1–3]. If a step-up transformer is placed after the filter, its leakage inductance can reduce the size of the second inductor leg or completely replace it [4]. Alternatively, the transformer can be put directly after the inverter, with the LCL filter on the transformer secondary side. This will reduce the ampacity of the filter inductors, reducing both size and losses in the filter. The drawback of this is an increased voltage transient stress on the transformer windings that has to be taken into account in the transformer design. However, the total efficiency of the system may be improved, and this topology could be considered for grid connection of renewable energy sources. Stray capacitance between windings, which normally is neglected at steady state, may play a more central role. Semiconductor switching into magnetic components is not unusual in power electronics, for example, the flyback converter. However, these circuits are based on ferrite cores, optimized for the switching frequencies in the system. Little research is found in the area of continuous pulse modulation into laminated steel-core transformers and its associated losses.

This paper presents a VSI with bipolar sinusoidal pulse-width modulation (SPWM) directly connected to a three-phase power transformer and the measured total magnetization losses. To get a reference case, the transformer is magnetized with 50 Hz at different voltage levels. The transformer saturation curve and magnetizing resistance are derived as functions of the induced voltage. A simulation model of the system is developed and uses the measured data at 50 Hz to set the internal parameters. Experiments with variations in DC voltage level and modulation index are conducted. The simulation model is verified, and the magnetization losses are evaluated for different amplitude modulations.

2. Theory

Starting from Faraday's law, the Magnetic field intensity, $\overline{B}$, in the transformer core is derived from the induced voltage $\overline{V}_{\text{ind}}$

according to

$$B(t) = \frac{1}{NA}\int_0^t V_{\text{ind}}(t)\,\mathrm{d}t + B_r(0), \tag{1}$$

where N is the number of winding turns, A is the average cross-sectional area of the magnetic core, and $B_r(0)$ is the remanescent flux of the magnetic core. B is coupled to the magnetic field strength $\overline{H}$ according to

$$\overline{H} = \mu_r \mu_0 \overline{B}, \tag{2}$$

where $\mu_0 = 4\pi \cdot 10^{-7}\,V\,s/Am$ is the magnetic permeability of free space, and μ_r is the relative permeability constant, a nonlinear material-dependent parameter. If the magnetizing current $\overline{I}_m$ is known, $\overline{H}$ is calculated by

$$H(t) = \frac{\overline{I}_m}{N\mathfrak{R}}, \tag{3}$$

where $\mathfrak{R}$ is the magnetic reluctance of the core.

The core losses of any magnetic component are distributed between eddy current losses, excess eddy current losses, and hysteresis losses. All of these have nonlinear behaviour and depend on the magnetic material properties and the operating temperature, as well as the waveform and frequency of the induced voltage. There are two established ways of calculating the core losses, either from the theoretical derivations of each loss separately [5, 6] or empirically by the Steinmetz equation [7] as follows:

$$P = kf^{\alpha}B^{\beta}, \tag{4}$$

where k is a material constant and f is the frequency of the magnetic flux. The exponents α and β are nonlinear functions of the other parameters.

Steinmetz equation is preferable, since the needed parameters usually are provided by the manufacturers data sheets. However, it is limited to sinusoidal waveforms and specific operating conditions. Also, having nonsinusoidal waveforms may cause large deviations in the loss calculations [8–10]. Splitting the waveform into its Fourier components and calculating the losses at the individual frequencies does not give very accurate results due to the complex interdependence of the losses. Also, it is difficult to accurately obtain all the Steinmetz parameters for a broad range of frequencies. Modifications of the Steinmetz equation are found in, for example, [11]. In [12, 13], attempts have been made to generalize the core loss calculations for an arbitrary current shape.

The classical eddy current losses may be described by [14]

$$P_{\text{eddy}} = \frac{A}{8\pi\rho}\left(\frac{dB(t)}{dt}\right)^2, \tag{5}$$

while hysteresis losses are calculated by integrating the B-H-curve over one cycle as

$$P_{\text{hys}} = f\int_t^{t+T} B(t)\,H(t)\,\mathrm{d}t. \tag{6}$$

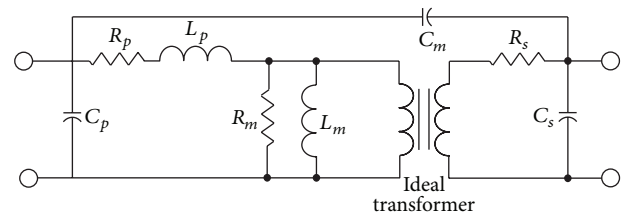

Figure 1: Transformer high-frequency equivalent circuit.

The high-frequency model of a single-phase transformer is shown for the no load case in Figure 1. R_p and R_s are the winding resistances on the primary and secondary sides, respectively. Only the leakage inductance of the primary side, L_p, is included, since the secondary leakage flux is so small at no load. Publications on high-frequency modelling of power transformers mainly discuss the pulse response, as in, for example, [15].

The internal stray capacitances of the windings, C_p and C_s, as well as the stray capacitance between the primary and secondary winding, C_m, become very important in transient analysis. Detailed calculations on transformer stray capacitance is found in [16, 17]. The stray capacitance will be in the order of pF and is neglected throughout this work since it will not significantly alter the power dissipation.

The magnetizing resistance, R_m, represents the total core losses, and the magnetizing inductance, L_m, represents the magnetic flux in the core. Assuming sinusoidal input voltage, both R_m and L_m, for rated voltage and frequency of the transformer, can be found in the manufacturers data sheets. However, these results are not valid at voltages and frequencies deviating from the transformer ratings.

One common way of inverter control signal generation is by the sinusoidal pulse-width modulation (SPWM), where a sinusoidal reference signal is compared with a carrier waveform. Assuming symmetry, the SPWM output voltage of the inverter can be expressed by its Fourier components according to

$$V_{\text{SPWM}}(t) = \sum_{h=1}^{N} V_h \sin(h\omega t), \tag{7}$$

where h is the order of the harmonic. Assuming ideal switching with no delay time between switching states, the three-phase rms voltage of the fundamental frequency is calculated as (remembering the neutral is floating)

$$V_1 = \frac{V_{\text{DC}}}{\sqrt{2}} m_a \tag{8}$$

and may be considered independent of the switching frequency, f_s. Equation (8) is only valid in the linear range (0-1) of the amplitude modulation index, m_a. In SPWM, the significant output harmonics are predominantly grouped around multiples of f_s [18].

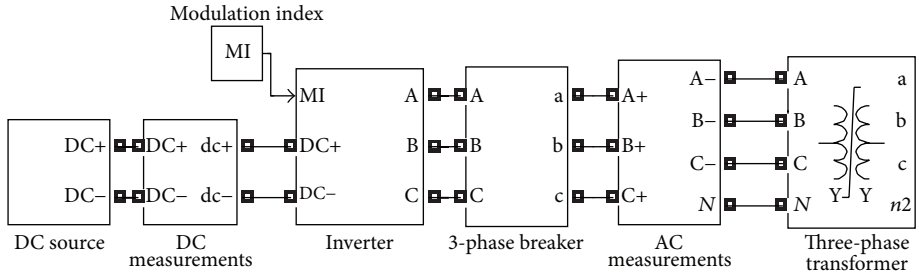

Figure 2: Simulink model block diagram.

The rms voltage of the unfiltered V_{SPWM} can be calculated as

$$V_{\text{SPWM,rms}} = \sqrt{\sum_{h=1}^{N} V_{h,\text{rms}}}, \tag{9}$$

where rms values of the harmonics can be found in [18].

3. Simulations

The Simulink model of the system is illustrated in Figure 2. Each block, from left to right, is described in the following. In the model, an ideal DC voltage source is used, and the DC power drawn by the circuit is measured. The three-phase inverter uses six IGBT blocks in parallel with six free-wheeling diodes. Device parameters come from the data sheets for the devices used in the experimental set-up. The inverter is operated with SPWM control, comparing a perfect sine wave to a sawtooth carrier wave at $f_s = 6$ kHz.

To limit the inrush currents at start-up and allow the system to settle, damping resistors are initially connected in series with the inverter and the transformer. When the system has settled, in approximately 100 ms, a breaker is closed to bypass the resistors in the circuit.

The three-phase transformer is modelled as three linear transformers in accordance with the equivalent model shown in Figure 1, but neglecting the stray capacitance of the system. The transformer parameters from Table 1 are used as input together with the saturation curve interpolated in Figure 4. A detailed description of the saturation model used is found in [19, 20]. By estimation of $V_{\text{SPWM,rms}}$ from (9), a value of R_m is taken from the interpolated curve in Figure 3. R_m is kept constant for each full simulation together with m_a and the DC-link voltage.

The model does not include any temperature dependence, since the power loss is considered low for the no load tests. Also, the model assumes uniformly distributed flux in the core.

Initially, the transformer at no load is magnetized with the 50 Hz grid voltage at different voltage levels. The total losses are shown in Table 2. From this, a value of R_m is obtained, as shown in Figure 3. A curve fit is done by piece-wise shape preserving cubic interpolation (pchip). This curve is used as simulation input, using the derived rms value of the inverter voltage from (9). R_m varies widely over the measured range due to the magnetic properties and the transformer design. The interpolated curve is considered valid within the range of measured data points, that is, for $V_{\text{rms}} \in [0 \quad 1.15]$. The value of the magnetizing resistance represents for both hysteresis losses and eddy current losses.

To get the saturation curve of the transformer, no load phase currents and voltages were measured at various voltage levels. The induced voltage is proportional to the induced flux, and they coincide at 1 pu. The results are used to plot the upper part of the saturation curve, shown in Figure 4. Symmetry is assumed for the lower quadrant, and the saturation curve is extrapolated by the use of an arctan function.

Table 1: Transformer characteristics.

Power rating	80 kVA
Voltage ratio	345 V Y/1 kV Y
R_p	0.0030535 pu
R_s	0.0096 pu
L_p	0.19858 pu
L_s	0.57303 pu
L_m (50 Hz, 1 kV)	500 pu
R_m (50 Hz, 1 kV)	89 pu

Table 2: Magnetization losses at normal 50 Hz magnetization.

V_s [pu]	Experimental P_{loss} [pu]	Simulated P_{loss} [pu]
0.130	0.00010	0.000088
0.425	0.00040	0.00042
0.700	0.0011	0.0011
1.00	0.0037	0.0037
1.15	0.0098	0.0098

4. Experimental Set-Up

A single-line diagram of the experimental set-up is depicted in Figure 5. The rectified grid voltage is used as DC source in the experiment. By changing tap on the tap transformer, different DC levels are obtained. The DC-capacitor bank is rated at 19 mF. Additional capacitors with small equivalent series resistance (ESR) are also used to reduce the high-frequency ripple in the DC voltage. The three-phase inverter consists of six 400GB126D IGBTs with 2SC0108T2Ax-17 Concept Driver Boards, as shown in Figure 6(a). Bipolar

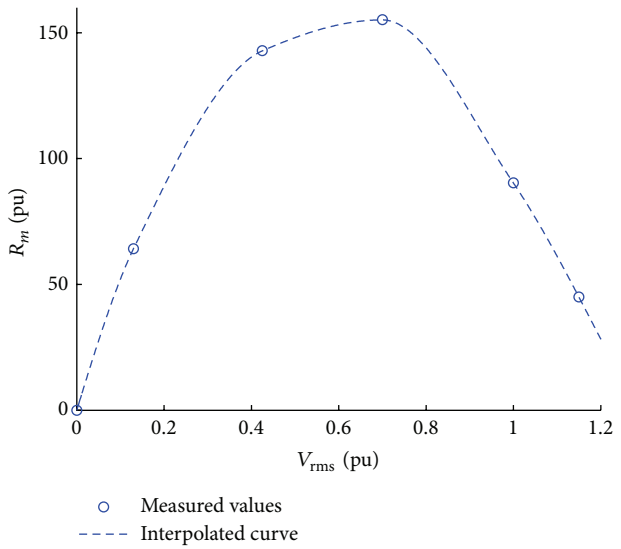

Figure 3: Magnetizing reluctance versus V_{rms}.

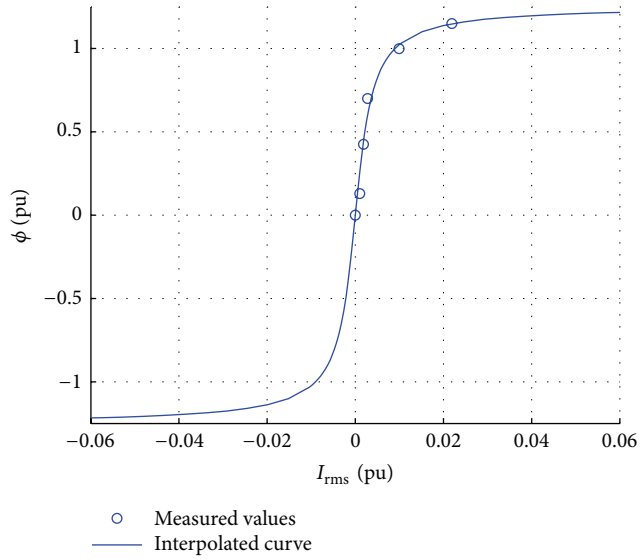

Figure 4: Saturation curve used in simulations.

SPWM control is used with a sawtooth wave as the carrier waveform. The switching frequency, f_s, is set to 6 kHz, and the delay time between switching transitions is set to 2.5 μs. The inverter is connected to the low side of the YY 345/1 kV 80 kVA three-phase transformer shown in Figure 6(b). The neutrals of the transformer are left floating to avoid the flow of zero sequences. The transformer ratings at rated voltage and frequency are displayed in Table 1. Base power and base voltages used for per-unit calculations are taken from this. The three-phase voltages into the magnetized transformer are measured by high-frequency differential voltage probes SI-9002, with an accuracy of ±1%. To calculate the total power losses dissipated in the transformer for no load. The three-phase currents are measured with current clamps Fluke i310s, with an accuracy of ±2%. Measurements are sampled at 400 kHz, and the power dissipation per phase is calculated. Transformer temperature was not measured during the experiment.

5. Results and Discussion

Transformer data at rated voltage and 50 Hz frequency are given by the manufacturer data sheet. The transformer is magnetized in no load at voltages lower than rated for 50 Hz. Measured and simulated power losses are displayed in Table 2. Simulations are performed for the same set-up, using the saturation curve in Figure 4 and the value of R_m in Figure 3. The winding parameters given for rated voltage are assumed constant and independent of frequency for the entire voltage range at no load. There is very good agreement between simulations and experiments, and the magnetization losses are slightly less than 1% of the transformer rating at rated voltage.

The saturation curve shows the classical trendline of an arctan function and will not affect magnetization losses significantly, as the winding resistance is small. For more accurate simulations, more measured values of R_m are

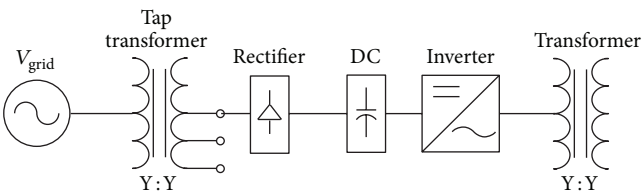

Figure 5: Single-line diagram of the experimental set-up. Magnetization losses are measured on the transformer to the right.

required to give a better curve fit, especially at lower and higher voltage levels, where the curve is expected to stagnate. The approximated value of R_m puts a limit on the simulation range, which is kept within (0.2–0.8). The estimation of R_m is of course not exact, as it represents frequency-dependent eddy current losses and hysteresis losses. However, it will give a fair approximation of the system losses that is simple to implement.

Next, the model is used to simulate the magnetization losses with the nonfiltered inverter. $V_{\text{SPWM,rms}}$ is estimated for the different scenarios and used to get an average value of R_m. The true value of $V_{\text{SPWM,rms}}$ will deviate slightly from the estimated, as the voltage will be partially filtered by the transformer. The measured magnetizing current and induced phase voltage for one phase are displayed in Figure 4. In Figure 7(a), 50 Hz magnetization is shown. In Figure 7(b) the same fundamental voltage is induced using the SPWM-controlled inverter instead. Excluding switching frequency harmonics, the harmonic content of the two currents is very similar. However, the inverter current is almost twice as large as the 50 Hz current. The pulsed current does not induce magnetic flux in the magnetic core as efficiently as the 50 Hz current. Thus it has to be higher for the same flux, and the magnetic losses will be higher.

The DC voltage is set at three different levels, and the total power loss is measured, while the amplitude modulation

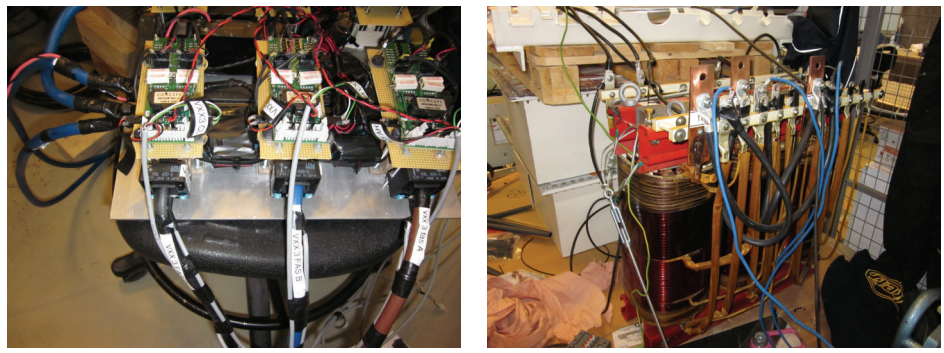

(a) (b)

Figure 6: (a) Inverter, (b) three-phase transformer.

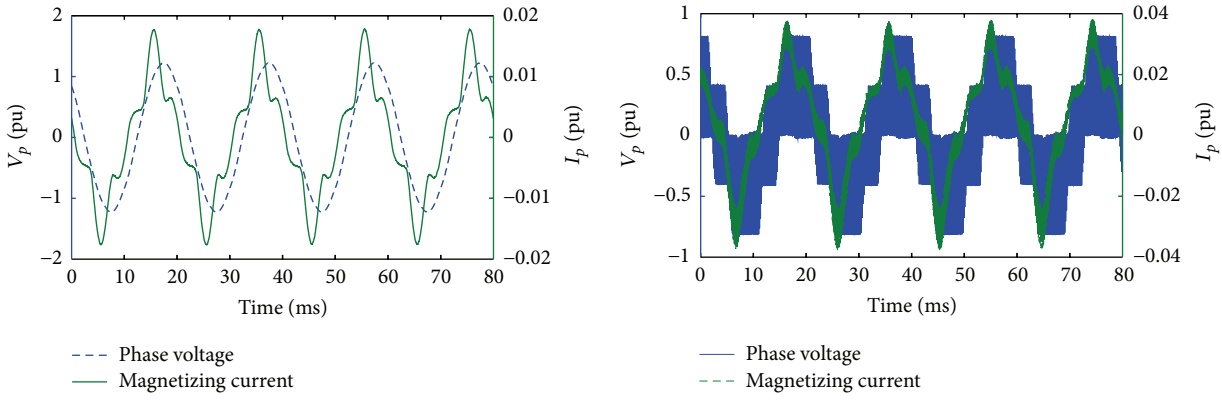

(a) (b)

Figure 7: (a) Magnetizing current for 50 Hz, (b) magnetizing current for SPWM.

is varied. In Figure 8(a), the DC level is set to 145 V, in Figure 8(b) is set to 335 V, and in Figure 8(c) is set to 550 V, respectively. There is rather good agreement between simulations and experiments. The limitation of the model is the estimation of R_m by the use of $V_{\text{SPWM,rms}}$. For $V_{\text{DC}} = 145$ V, the simulated power is slightly higher than the experimental. This is also true for $V_{\text{DC}} = 550$ V. Here, the "knee" seen in the power curve is sharper in the experiments than the simulations. The possible explanation to this is the approximation of the R_m curve and using $V_{\text{SPWM,rms}}$ to represent the voltage input. A squared interpolation of the R_m curve could possibly give more accurate simulation results.

For the lower DC voltages, the power loss is approximately proportional to m_a, whereas it starts to increase with the square of m_a for the highest voltage. This is reasonable, since the losses increase with the square of the rms voltage. Also, the magnetic core will be in its linear region for lower voltages and magnetic fluxes, whereas it will go into partial saturation, as the induced voltage is increased. In Figure 8(c), it can be seen that the losses at an induced voltage of 0.8 pu are less than half the losses at 1 pu. This indicates that a significant improvement in the magnetization losses can be made by shifting the operating point for the transformer, which is equivalent to having a larger core at nominal voltage. When the transformer is SPWM-magnetized at its rated voltage, ($V_{\text{DC}} = 550$ V, $m_a = 1$), the magnetization losses are ten times higher than the 50 Hz magnetization at rated voltage given in Table 2.

In Figure 9, the overlap of the experimental results are plotted from the data in Figure 8. The same fundamental voltage output is obtained for different DC levels by varying the amplitude modulation. The corresponding losses at 50 Hz-magnetization are also plotted as a reference. Nonfiltered inverter magnetization always dissipate higher losses in the transformer compared to the sine wave. This makes perfect sense, since the transformer is optimized for this frequency. Also, both eddy current losses and hysteresis losses increase with frequency. In this experiment, the lower DC voltages are not sufficient to give the transformer full magnetization, as can be seen in Figure 9. However, there is a general trend that the losses increase for higher DC voltages with the same V_s. This is in agreement with that $V_{\text{SPWM,rms}}$ increase for an increased V_{DC} while maintaining the product $m_a \cdot V_{\text{DC}}$ constant. At rated voltage, least magnetization losses are obtained for the lowest possible V_{DC}, that is, when $m_a = 1$.

6. Conclusions

In this paper the losses of a three-phase power transformer, magnetized by a nonfiltered inverter, have been evaluated.

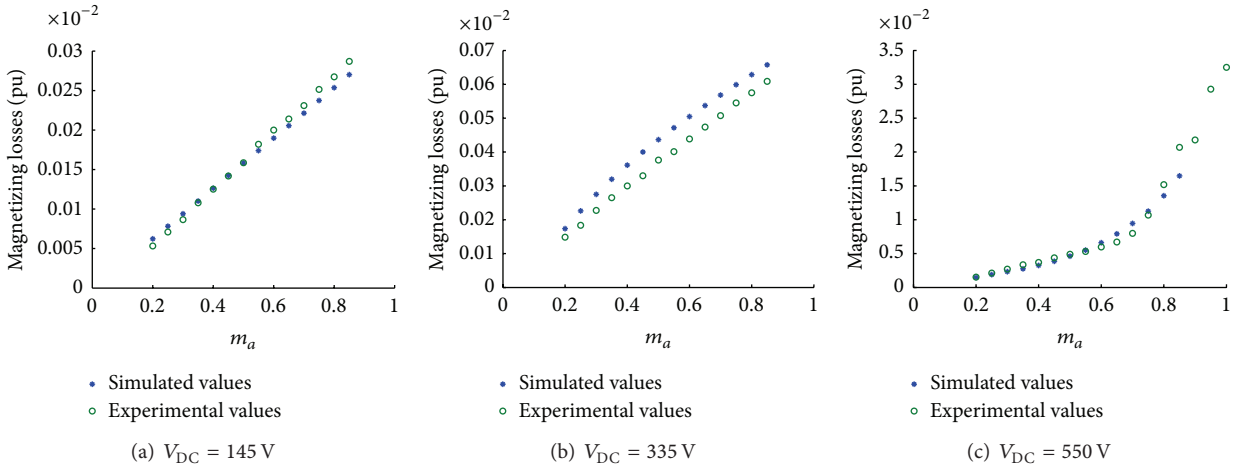

Figure 8: Comparison of magnetization losses between simulations and experiments, at different values of V_{DC}.

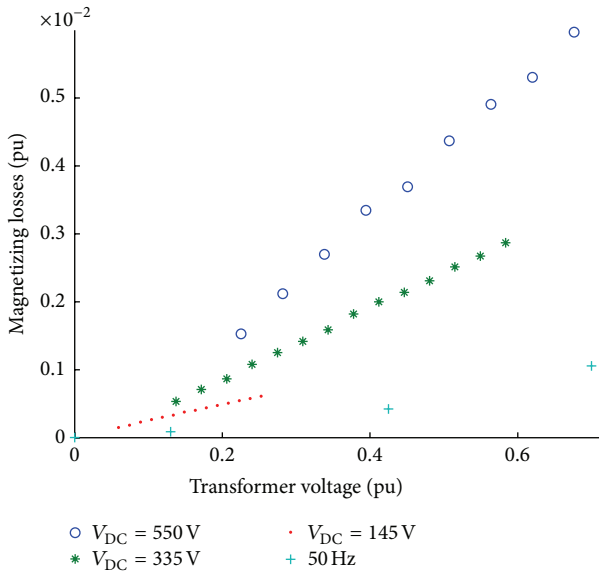

Figure 9: Magnetization losses for the same transformer voltage with different V_{DC}.

A simulation model has been developed based on the measured parameters of the system. The total core losses are lumped into an equivalent magnetizing resistance based on the rms value of the induced voltage, and this method shows good resemblance with the experimental measurements. For the studied cases, the magnetization losses are always higher using direct VSI magnetization compared to normal 50 Hz voltages. For VSI magnetization, the losses increase rapidly close to the transformer nominal voltage. This is because the switched voltage waveform pushes the transformer to operate more in its saturated region. At rated voltage, the magnetization losses are approximately ten times higher for SPWM than for normal 50 Hz. The results show that by shifting the transformer operating point, the magnetization losses can be significantly reduced.

To minimize the magnetization losses for a given secondary voltage, the amplitude modulation should be kept as high as possible. The increased transformer losses have to be evaluated in conjunction with decreased LCL filter losses to evaluate the total system efficiency in this set-up compared with more conventional topologies.

References

[1] H. R. Karshenas and H. Saghafi, "Performance investigation of LCL filters in grid connected converters," in *Proceedings of the IEEE PES Transmission and Distribution Conference*, 2006.

[2] T. C. Y. Wang, Z. Ye, G. Sinha, and X. Yuan, "Output filter design for a grid-interconnected three-phase inverter," in *Proceedings of the IEEE 34th Annual Power Electronics Specialists Conference*, pp. 779–784, June 2003.

[3] E. Twining and D. G. Holmes, "Grid current regulation of a three-phase voltage source inverter with an LCL input filter," *IEEE Transactions on Power Electronics*, vol. 18, no. 3, pp. 888–895, 2003.

[4] M. Prodanović and T. C. Green, "Control and filter design of three-phase inverters for high power quality grid connection," *IEEE Transactions on Power Electronics*, vol. 18, no. 1, pp. 373–380, 2003.

[5] W. Roshen, "Ferrite core loss for power magnetic components design," *IEEE Transaction on Magnetics*, vol. 27, no. 6, pp. 4407–4415, 1991.

[6] M. L. Hodgdon, "Applications of a theory of ferromagnetic hysteresis," *IEEE Transaction on Magnetics*, vol. 24, no. 1, pp. 218–221, 1988.

[7] C. P. Steinmetz, "On the law of hysteresis," *American Institute of Electrical Engineers Transactions*, vol. 9, pp. 3–64, 1892.

[8] A. Boglietti, P. Ferraris, M. Lazzari, and F. Profumo, "Iron losses in magnetic materials with six-step and PWM inverter supply," *IEEE Transactions on Magnetics*, vol. 27, no. 6, pp. 5334–5336, 1991.

[9] M. Amar and F. Protat, "Simple method for the estimation of power losses in silicon iron sheets under alternating pulse voltage excitation," *IEEE Transactions on Magnetics*, vol. 30, no. 2, pp. 942–944, 1994.

[10] A. V. Bossche, V. C. Valchev, and G. B. Geoorgiev, "Measurements and loss model of ferrites with nonsinusoidal waveforms," in *Proceedings of the 35th IEEE Power Electronics Specialists Conference*, pp. 4814–4818, 2004.

[11] J. Reinert, A. Brockmeyer, and R. W. A. A. De Doncker, "Calculation of losses in ferro- and ferrimagnetic materials based on the modified Steinmetz equation," *IEEE Transactions on Industry Applications*, vol. 37, no. 4, pp. 1055–1061, 2001.

[12] M. Albach, T. Duerbaum, and A. Brockmeyer, "Calculating core losses in transformers for arbitrary magnetizing currents a comparison of different approaches," in *Proceedings of the 27th Annual IEEE Power Electronics Specialists Conference (PESC '96)*, pp. 1463–1468, January 1996.

[13] W. A. Roshen, "A practical, accurate and very general core loss model for nonsinusoidal waveforms," *IEEE Transactions on Power Electronics*, vol. 22, no. 1, pp. 30–40, 2007.

[14] E. C. Snelling, *Soft Ferrites: Application and Properties*, Butterworths, London, UK, 2nd edition, 1988.

[15] A. Morched, L. Marti, and J. Ottevangers, "High frequency transformer model for the EMTP," *IEEE Transactions on Power Delivery*, vol. 8, no. 3, pp. 1615–1626, 1993.

[16] H. Y. Lu, J. G. Zhu, and Y. Hui, "Experimental determination of stray capacitances in high frequency transformers," *IEEE Transactions on Power Electronics*, vol. 18, no. 5, pp. 1105–1112, 2003.

[17] J. Biela and J. W. Kolar, "Using transformer parasitics for resonant converters—a review of the calculation of the stray capacitance of transformers," *IEEE Transactions on Industry Applications*, vol. 44, no. 1, pp. 223–233, 2008.

[18] N. Mohan, T. Undeland, and W. Robbins, *Power Electronics—Converters, Applications and Design*, John Wiley & Sons, New Dehli, India, 5th edition, 2007.

[19] S. Casoria, G. Sybille, and P. Brunelle, "Hysteresis modeling in the MATLAB/Power System Blockset," *Mathematics and Computers in Simulation*, vol. 63, no. 3–5, pp. 237–248, 2003.

[20] J. G. Frame, N. Mohan, and T. Liu, "Hysteresis modeling in an electromagnetic transients program," *IEEE Transactions on Power Apparatus and Systems*, vol. 101, pp. 3403–3412, 1982.